Available online at www.sciencedirect.com
SCIENCE DIRECT®
Journal of Nuclear Materials 324 (2004) 116–124
journal of nuclear materials
www.elsevier.com/locate/jnucmat

Failure predictions for nuclear graphite using a continuum damage mechanics model

Z. Zou, S.L. Fok *, S.O. Oyadiji, B.J. Marsden

Manchester School of Engineering, University of Manchester, Manchester M13 9PL, UK

Received 16 December 2002; accepted 5 September 2003

Abstract

A failure model for nuclear graphite is presented in the context of continuum damage mechanics. It relates tractions to the relative displacements at an interface where cracking may occur. Both the stress-based and fracture-mechanics-based failure criteria are included in the model to construct a damage surface which shrinks in the stress space as damage develops. Damage initiation is governed by the stress criterion and full formation of a crack by the fracture-mechanics criterion. The unified failure model can deal with failure under both regular and singular stress concentration conditions. Numerical predictions for tension of L-shape and channel-section graphite specimens of different corner radius, including sharp corner, have been performed. The predicted failure loads are in good agreement with available experimental data. This indicates that the present failure model is suitable for graphite material.

1. Introduction

The cores of graphite-moderated, gas-cooled reactors normally compose of many graphite components joined together by a system of graphite keys and keyways. Internal shrinkage and thermal stresses generated during operation may eventually lead to crack initiation from the keyway corners, which act as stress concentrations (singular in the case of sharp corner), and subsequent crack propagation may cause component failure.

Nuclear graphite is a brittle, polygranular material that is stronger in bending than in tension and stronger in compression than in bend [1]. Therefore, as with other brittle materials, failure of nuclear graphite is not only a function of component geometry and size but also of loading mode. For this reason engineers involved in reactor designs or reactor lifetime extension have had to rely on full-sized component testing to determine failure loads. Failure stresses at the keyway corners are estimated using finite element analysis and are taken as a measure of the components' strength. These are subsequently modified to account for irradiation effects and may then be used for life predictions. Unfortunately this is not practical for the case of sharp corners or in the case of small radii of similar dimensions to the graphite grain size. Therefore, at present, in the absence of satisfactory graphite failure model, various approximations have to be made when predicting time to failure for various core components.

In existing graphite components, the fillet radius at the keyway corner varies and can be very small or may have a faceted shape. Indeed the corner radii may be of a similar dimension to the granular structure of the graphite material. Consequently, stress concentration may vary from regular to singular at the keyway root. Both experimental and theoretical work has been carried out to investigate structural integrity issues related to graphite moderator components. However, at present, the assessment of the failure of these components is based on relatively simple approaches, e.g. critical stress which is defined as the maximum stress at the keyway root surface when the specimen fails. Such a critical stress is root radius dependent.

* Corresponding author. Tel.: +44-161 275 4327; fax: +44-161 275 4328.
E-mail address: alex.fok@man.ac.uk (S.L. Fok).

0022-3115/$ - see front matter © 2003 Elsevier B.V. All rights reserved.
doi:10.1016/j.jnucmat.2003.09.005

Many failure models have been developed in the literature for predicting strength of structures containing stress concentrations. The strength predictions in the case of non-singular stress concentrations, generated by holes or round cornered notches, are usually based on classical stress-based failure criteria [2–4]. A characteristic length is proposed in these models. Failure is assumed to occur when the average stresses over the characteristic length satisfy a maximum-stress failure criterion. Instead of the average stresses, point stresses may also be used which are defined as those at a distance of the characteristic length away from the hole or notch surface. These criteria strongly depend on the characteristic length itself, which can sometimes be arbitrary or ambiguous.

Singular stresses may exist at sharp notch tips with the order of stress singularity depending on the notch angle. Use has been made of critical stress intensity as a criterion for fracture initiation at notch tips with a non-zero angle [5]. It was shown in [5] that, although the critical stress intensity obtained from the specimens of four different notch depths varied only slightly, it was notch-angle dependent. This method may therefore not be able to predict subsequent crack propagation. If the notch angle reduces to zero or if there is a pre-existing crack at the notch tip, the problem becomes that of a classical crack. Fracture mechanics can then be applied directly.

The cohesive zone model is often employed to simulate crack propagation [6,7]. The model relates tractions to the relative displacements at an interface where a crack may occur. A constitutive law for the tractions and displacements is employed. There is a maximum (critical) value for the traction on the constitutive curve. When the area under the constitutive curve is equal to the critical fracture energy or when the relative displacement reaches a critical value, the traction is reduced to zero and free crack surfaces are formed. The interfacial potential energy function has also been used to derive the interfacial constitutive law [8]. Several traction/displacement curves, e.g. exponential [9], bilinear [10] and trapezoidal [11] have been employed in the literature. The cohesive zone model can be easily implemented into an existing FE code via an interface element.

The cohesive zone model has also been applied to blunt stress concentration by Smith [12,13]. It is assumed that the stress within the cohesive zone remains constant at a critical value until the displacement attains a critical value, then the stress is assumed to fall abruptly from the critical value to zero. This is similar to the classical elastic–perfectly plastic traction/displacement curve used by Dugdale [14] to consider the plastic fracture in steel sheets containing slits.

In this paper, a phenomenological failure model is presented in the context of continuum damage mechanics. It is originally developed by Zou et al. [15] to deal with interfacial delamination in composite laminates. Its application is extended to graphite material in the present paper. In this failure model, a damage parameter is employed and the interfacial constitutive law is expressed as a function of the damage parameter to take account of the effects of damage. Both the conventional stress-based and fracture-mechanics-based failure criteria are included in the new failure model to construct a damage surface. Damage initiates when the stress-based criterion is first satisfied. As damage develops, the damage surface shrinks in the stress space, leading to a softening interfacial constitutive law. A crack is fully formed when the work done by the tractions meets the fracture-mechanics-based criterion.

The new failure model can be viewed as an extension or generalisation of the cohesive zone model, in that it coupled together the effects of mode-I and mode-II loadings and all the traction/displacement curves mentioned above can be derived from the combined stress-based and fracture-mechanics-based failure criterion.

The failure model was implemented into the commercial finite element code ABAQUS [16] via the user subroutine user element (UEL). Numerical analysis was carried out to assess the strength of L-shape and channel-section graphite specimens. Effect of the root radius, i.e. from a sharp corner to relatively large radii, on the failure load was also investigated. Good agreement was achieved between the predictions and available experimental data. This indicates that the present failure model is suitable for graphite material. Sensitivity of the predicted failure loads to the material strength and fracture energy is also discussed.

2. Model description

An interface is introduced into the continuum solids at the position where potential crack surfaces may form. It has no thickness and perfect connection exists across the interface before damage initiation. As the load level increases, damage, e.g. micro-cracks, may initiate at the stress concentration site (e.g. crack or notch tip) and gradually develop along the interface. This is illustrated in Fig. 1 schematically. A damage parameter ω is introduced and the interfacial constitutive law is expressed as functions of the damage parameter to take account of the effects of damage as follows:

$$\tau_i = k_i^0(1-\omega)\delta_i \quad (i=1,2), \tag{1}$$

where τ_i are the tractions on the interface, δ_i the relative displacement components across the interface, and k_i^0 are constraint stiffnesses of the interface. Subscript 1 indicates the direction normal to the interface, and 2 the direction along the interface. The damage parameter ω

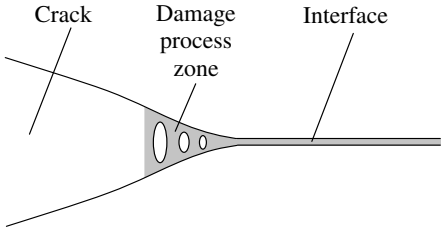

Fig. 1. Crack, damage process zone and interface.

is a non-dimensional measure which describes the extent of damage at a local point on the interface. For instance, $\omega = 0$ indicates no damage and $\omega = 1$ signifies a fully cracked state.

The initial interface stiffnesses k_i^0 act as penalty parameters to simulate a real connection between two neighbouring solids before damage initiation. They should be large enough to provide reasonable connection but small enough to avoid numerical problems in a finite element analysis. A reasonable choice for the interface stiffness is suggested to be as follows [17,18]:

$$k_i^0 = k\tau_{ic}, \quad k = 10^5\text{–}10^7 \text{ mm}^{-1}, \tag{2}$$

where τ_{1c} and τ_{2c} are the tensile and shear strengths of the continuum material.

The damage process in the context of continuum damage mechanics involves two aspects, the initiation and growth of damage. The concept of a damage surface, similar to the yield surface in plasticity, has been introduced for establishing damage evolution laws in continuum damage mechanics. A damage surface is therefore constructed as follows:

$$F(\tau_i, G_i) = f_s(\tau_i) + f_g(G_i) - 1 = 0, \tag{3}$$

where f_s is a stress-based failure criterion function and f_g a fracture-mechanics-based criterion function, which are available in the literature for different considerations, e.g.

$$f_s = \frac{\tau_1^2}{\tau_{1c}^2} + \frac{\tau_2^2}{\tau_{2c}^2} \quad \text{and} \quad f_g = \frac{G_I}{G_{Ic}} + \frac{G_{II}}{G_{IIc}}, \tag{4}$$

while G_{ic} $(i = I, II)$ are the critical values of the individual energy release rates G_i $(i = I, II)$ of the material, with

$$G_i = \int_0^{\delta_i} \tau_i \, d\delta_i \quad (i = I, II \text{ or } 1, 2). \tag{5}$$

Other forms for these failure criteria functions may be easily included in the model if required.

The damage surface combines both the stress-based and fracture-mechanics-based failure criteria. Since the initial stiffnesses of the interface are chosen to be very large, relative displacements δ_i are negligible in the early stage of loading, so are G_i and f_g as a result. Damage initiates at an intact interface only if the stress-based criterion $f_s = 1$ is satisfied. As damage develops, stiffness of the interface degrades, resulting in quick increment in δ_i, G_i and f_g. The damage surface therefore shrinks in the stress (interfacial traction) space. Formation of fully cracked surfaces requires that the fracture-mechanics-based criterion $f_g = 1$ is also satisfied, leading to a vanished damage surface in the stress space, i.e. zero tractions at the interface.

When the damage surface is exceeded, i.e.

$$F(\tau_i, G_i) = f_s + f_g - 1 > 0, \tag{6}$$

then damage initiates or develops. An infinitesimal change of the damage state at the interface as a result of an infinitesimal change of tractions requires the satisfaction of the following equation so that the tractions, relative displacements and damage parameter remain on the damage surface, Eq. (3), i.e.

$$dF = \sum_{i=1}^{2} \left(\frac{\partial F}{\partial \tau_i} d\tau_i + \frac{\partial F}{\partial G_i} dG_i \right) = 0. \tag{7}$$

Making use of Eqs. (1), (5) and (7), the incremental interfacial constitutive law and damage evolution law can be obtained in terms of incremental relative displacements as [15]

$$d\tau_i = (1 - \omega) k_i^0 \, d\delta_i - k_i^0 \delta_i \sum_{j=1}^{2} C_j \, d\delta_j \tag{8}$$

and

$$d\omega = \sum_{i=1}^{2} C_i \, d\delta_i, \tag{9}$$

respectively, where

$$C_i = \left[\frac{\partial F}{\partial \tau_i} (1 - \omega) k_i^0 + \frac{\partial F}{\partial G_i} \tau_i \right] \Big/ \sum_{j=1}^{2} \frac{\partial F}{\partial \tau_j} k_j^0 \delta_j. \tag{10}$$

When the interfacial stresses are within the damage surface, i.e.

$$F(\tau_i, G_i) = f_s + f_g - 1 < 0, \tag{11}$$

no damage development can occur, thus

$$d\omega = 0 \tag{12}$$

and the incremental constitutive law becomes

$$d\tau_i = k_i^0 (1 - \omega) \, d\delta_i. \tag{13}$$

This situation may happen in the case of low stress level or local unloading.

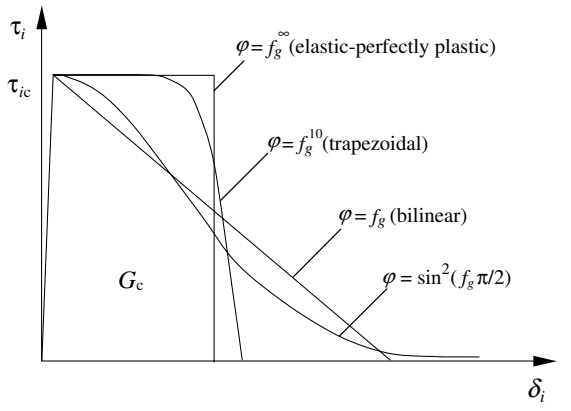

Fig. 2. Traction/relative displacement curves based on different damage surfaces.

If failure criterion functions f_s and f_g are expressed in the forms in Eq. (4), a typical bilinear traction/relative displacement curve for the single mode case can be obtained, as shown in Fig. 2 (with $\varphi = f_g$). As the relative displacement increases from zero, the traction increases linearly. Once the stress-based failure function f_s reaches unity, damage initiates. As relative displacement continues to increase, damage develops while traction decreases. When the fracture mechanics based failure function f_g equals unity, the damage parameter ω reaches unity at the same time. The traction is reduced to zero and complete crack surfaces are formed.

In general, the damage surface can be constructed even as follows:

$$F(\tau_i, G_i) = f_s(\tau_i) + \varphi(f_g) - 1 = 0, \tag{14}$$

where φ is a monotonically increasing function of f_g satisfying $\varphi(0) = 0$ and $\varphi(1) = 1$. Fig. 2 shows different constitutive relationships by choosing different forms of φ for the damage surface. Suppose $\varphi = f_g^n$, then the bilinear curve is obtained when $n = 1$. Increasing n reduces the shrinkage rate of the damage surface, causing the traction to decrease very slowly in the early stage after damage initiation. However, the energy dissipation rate will increase and the traction decrease quickly in the later damage state. A trapezoidal curve is thus generated when $n = 10$. If n is very large, the 'elastic–perfectly plastic' curve can be expected. If the sinusoidal function is adopted, smooth curves are usually produced which are asymptotic to the displacement axis. These curves are often found in the literature for the cohesive models.

An interface element was developed to implement this continuum damage mechanics model into the commercial finite element code ABAQUS [16] via the user subroutine user element (UEL). Dual coincident nodes along the likely crack path are required in the FE mesh. An interface element connects two solid elements and shares the nodes at the interface with them. The relative displacements across the interface at the position of the dual coincident nodes are simply the relative nodal displacements. Detailed formulations for the interface element can be derived in the normal way and will not be addressed here.

3. Numerical simulation of failure of graphite specimens

Many experiments have been conducted on graphite materials in previous investigations to simulate the failure at the keyway root of graphite moderator components. Among these, the tension tests on L-shape [19] and channel-section [20] specimens were analysed using the present model. Predicted results were compared with the experiments and parametric studies were also carried out to investigate some key factors. In this investigation $\varphi = f_g$, i.e. $n = 1$, was chosen for the bulk of the analysis.

In the FE analysis, 2D four-noded plane stress solid elements, CPS4 in ABAQUS [16], were employed to model the specimens. The smallest element has a length of 0.10–0.20 mm along the crack path which covers the full length of the possible fracture surface, determined by a preliminary finite element analysis of the positions of the maximum tensile stress σ_{max} prior to the main fracture analysis.

3.1. Tension of L-shape specimens

The geometry and loading of the L-shape graphite specimen is shown in Fig. 3. The specimens were 15 mm thick. Four corner radii ($r = 0$, 1, 2 and 4 mm, respectively) were tested. The load was applied through two metal pins which were inserted in the holes in the specimen. It is obvious that this is a mode-I fracture problem. The crack will appear at the corner and propagate along the horizontal broken line since the maximum principal stress is highest there. Interface elements of a length around 0.2 mm were created along this path. The pin was modelled as a rigid body and contact between the pin and specimen was also considered.

The properties for unirradiated, medium-grained, nuclear graphite material were used as given below:

$$E = 10 \text{ GPa}, \quad v = 0.2, \quad \tau_{1c} = 33 \text{ MPa},$$
$$G_{Ic} = 200 \text{ J m}^{-2},$$

where E and v are Young's modulus and Poisson's ratio, respectively.

To show the stress concentration at the corner, linear stress analysis was first performed without any consideration of damage. The maximum principal stress along the interface next to the corner is given in Fig. 4 at the load level equivalent to the failure load. As expected, a

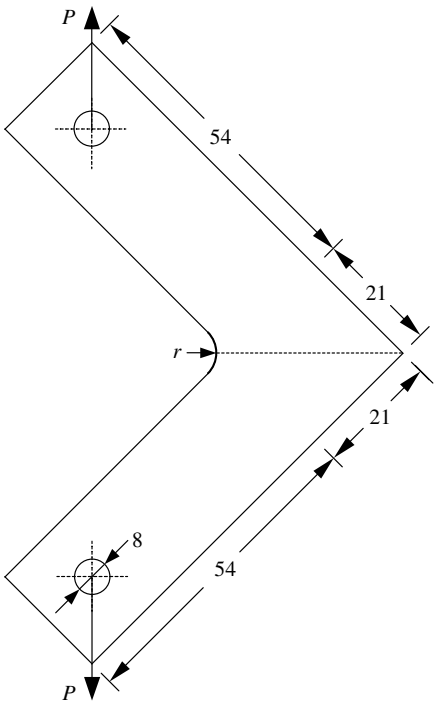

Fig. 3. Dimensions (mm) and loading of the L-shape specimen (15 mm thick).

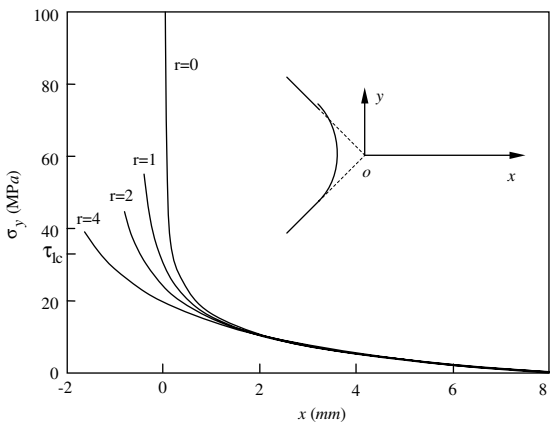

Fig. 4. Principal stress along the possible crack path next to the round corner at P_{cr}.

stress singularity was found at the sharp corner ($r = 0$). Both the stress concentration and stress gradient decrease as the corner radius increases.

However, no stress singularity can exist in the specimen when the damage model is included in the analysis. The stress cannot exceed the material strength τ_{1c} under the control of the damage surface (failure criterion). Typical stress distribution around the corner ($r = 2$ mm) is shown in Fig. 5 along with the predicted fully cracked surface. The crosses stand for the nodal positions of the interface elements. The damage zone covers 4–5 interface elements.

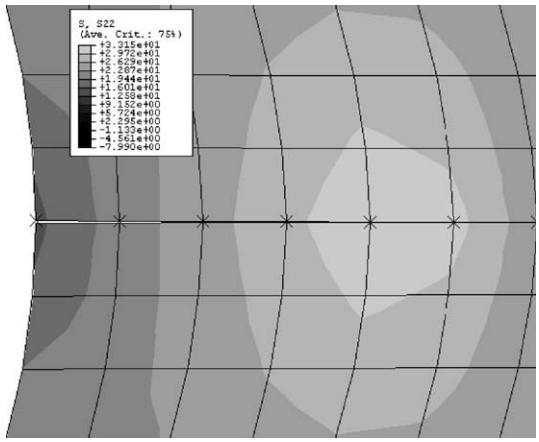

Fig. 5. Typical stress distribution and predicted crack around the corner ($r = 2$ mm).

Examination has been made to the predicted damage at the interface. The damage zone initiates at the corner surface and spreads into the interior of the specimen. The damage zone grows in a stable manner prior to the attainment of the maximum load. Once the fully formed crack appears at the corner surface, subsequent catastrophic crack propagation takes place, resulting in a sudden load drop. The larger the corner radius is, the quicker the crack propagates. Although no dynamic effect is included in the present analysis, the unstable crack propagation can be estimated from a sudden load drop in the load/displacement curve or the slow solution convergence rate.

The load/displacement (between two pins) curves are given in Fig. 6. As can be seen, the predicted curves are similar in shape to the experimental trace. There is initially a mainly elastic, linear rise up to a peak for the load, followed by a sudden drop caused by the unstable rapid crack propagation. Further displacement results in a gradual decrease in the load. The peak loads on these curves are apparently the failure loads of the specimens. The specimen with a small corner radius has a complete curve, because the maximum applied load is at a relatively low level and crack propagation speed is relatively slow during the unstable propagation period. During each displacement increment, very small in size, only a few interface elements break down and a converged solution can be reached. For the specimen with a large corner radius, the load level for damage initiation and formation of a full crack is much higher. Once the fully formed crack appears, it will grow much quicker and many interface elements break down in one increment.

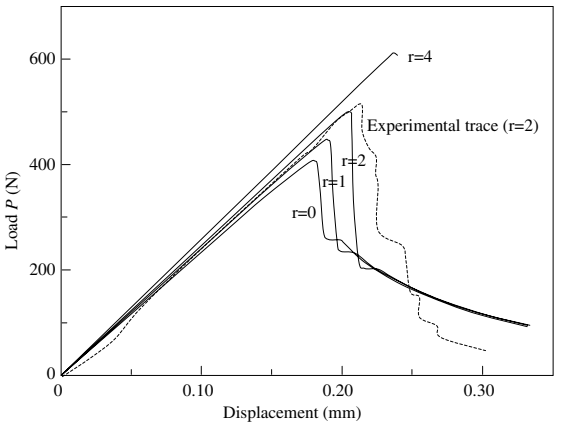

Fig. 6. Load/displacement curves for L-shape specimens.

Usually, no solution convergence can be achieved in this case.

Fig. 7 shows the comparisons between the predicted failure loads and the experimental results. The FE predictions are in good agreement with the experiments, except for the specimens with a corner radius of 1 mm. However, the prediction is still close to the lower bound of the experimental range. The sharper the corner, the severer the stress concentration and the lower the failure loads. The overall trend shows that the failure load increases as the corner radius becomes larger, showing an almost linear relationship between them in the given range.

A study of mesh effect on the prediction was performed on the four specimens. Two element sizes, around 0.2 and 0.1 mm respectively, were employed along the crack path. The relative differences between the predicted failure loads were less than 0.3 percent. Convergence has thus been achieved for these specimens.

To investigate the effect of possible initial flaw at the corner, an initial crack was assumed in the specimens and the failure analysis was repeated. The relationship between the predicted failure load (P_{cr}) and initial crack tip position (x) is given in Fig. 8, with all curves starting with a zero initial crack length and $x = 0$ being the position of the sharp corner root. An initial crack at the corner of a large radius significantly reduces the failure load. With the same crack tip position x in the specimen plane and $x < 0$, the larger the corner radius, and hence the longer the initial crack, the lower the failure load as a result. However, it is interesting to notice that the effect of the round corner almost vanishes once the initial crack reaches the position where the sharp corner root is. Consequently, a sharp corner is equivalent to an initial crack at a round corner with its tip at the sharp corner root position. These results also suggest that no initial flaws greater than 1 mm in length could have existed in the specimens tested. Otherwise, much smaller differences in the failure loads would have been found in the experiments.

The effects of the material strength and critical energy release rate on the failure load of the specimens were also investigated. Failure loads increase almost linearly with the increase of material strength and critical energy release rate, as shown in Figs. 9 and 10, with the rate of increase of the failure load of the specimens depending on the corner radius. Material strength has more effect on the specimens with a larger corner radius while the critical energy release rate has more effect on the specimens with small corner radii, especially the sharp corner. The sensitivity of the failure load to changes in the material strength and critical energy release rate for different corner radii is discussed further in the next subsection.

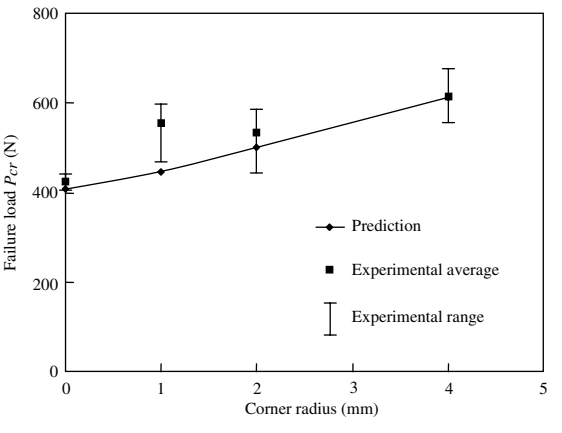

Fig. 7. Failure loads of the L-shaped specimens.

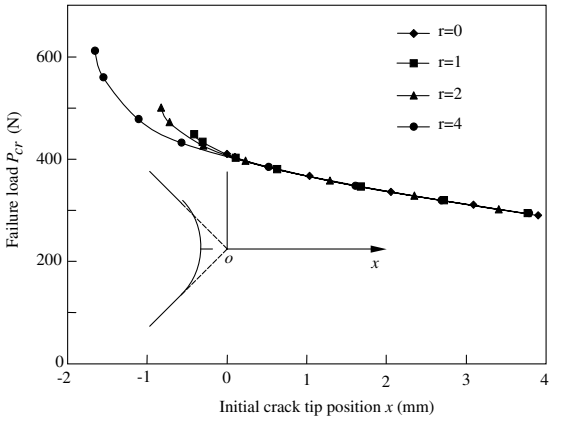

Fig. 8. Predicted failure loads of specimens with initial crack at the round corner.

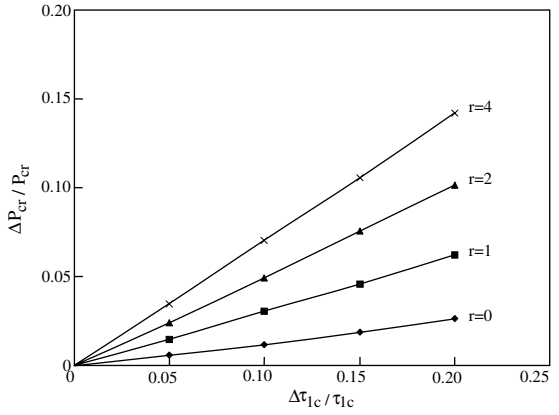

Fig. 9. Effect of material strength on failure load.

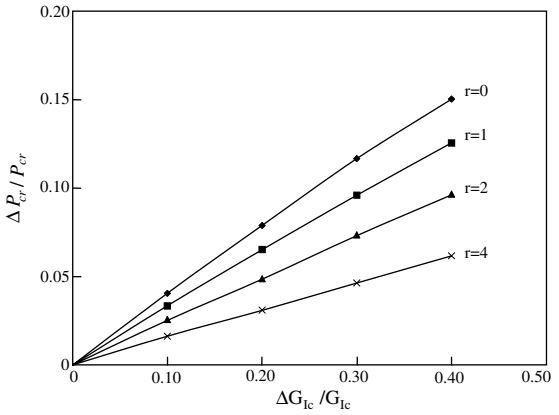

Fig. 10. Effect of critical energy release rate on failure load.

3.2. Failure of the channel-section specimens

The channel-section specimen shown in Fig. 11 can be considered as a typical part around a keyway in a real moderator brick slice. The thickness of the specimens was 10 mm and keyway corner radius $r = 0$, 1, 2, 4, 8 mm, respectively.

Due to the free surface at the corner, the maximum principal stress is in the local circumferential direction, the other two stress components, i.e. shear stress and the direct stress normal to the surface, vanish or are negligible near the corner surface. Cracking at the corner is mainly a mode I fracture problem. It is therefore assumed that crack initiates at the position of maximum circumferential stress around the corner and propagate along the local radial direction. The assumed crack path is shown in Fig. 11, marked by the broken line. A linear stress analysis was carried out first to determine the position of the maximum circumferential stress around

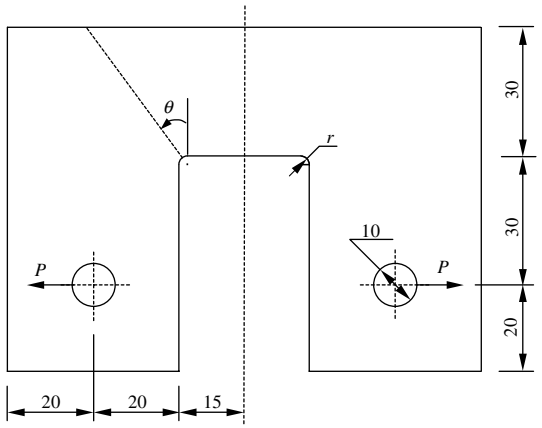

Fig. 11. Dimensions (mm) and loading of the channel-section specimen (10 mm thick) and assumed crack path (θ is angle of maximum circumferential stress).

the corner. The initial cracking angles (θ) for the different corner radii are given in Table 1. Interface elements were generated along this path in the FE model. Having a prescribed crack path meant that the cracking may not be a pure mode I problem away from the corner surface, effect of the minor mode-II component was considered through Eq. (4). Lacking in data, it was assumed that $\tau_{2c} = \tau_{1c} = 33$ MPa and $G_{IIc} = G_{Ic} = 200$ Jm^{-2}. An alternative approach has been adopted by Xu and Needleman [9]. In their work, interface elements were generated between all the neighbouring solid elements. The path of cracking can thus be predicted automatically by the model. However, a huge number of elements is required since the size of interface elements is very small. It is very computationally expensive, so this approach was not employed in the present analysis.

Similar to the L-shape specimens, crack propagation in the channel-section specimen is also unstable. Once a crack is fully formed at the corner surface, it grows all the way through the specimen with the applied load dropping rapidly. The predicted load/displacement curves are similar to those of the L-shape specimens and no longer presented here. It was, however, more difficult to fully capture the rapid load drop on the load/displacement curves for channel-section specimens than for the L-shaped specimens.

Fig. 12 shows the comparisons between the predicted failure load and experimental results. As can be seen, the FE predictions are in good agreement with the experiments. Once again, the overall trend from both the experiments and predictions shows an almost linear

Table 1
Cracking angle for the channel sections

r (mm)	0	1	2	4	8
θ (°)	36	31.5	27	22.5	16.25

relationship between the failure load and the corner radius in the given range.

The effect of corner radius on the sensitivity of specimen failure load to material strength and critical energy release rate is given in Fig. 13. In general, energy release rate is in proportion to the square of the applied load. Therefore, increase in the critical energy release rate is chosen to be twice that in material strength to make the predictions comparable. As the corner radius gets larger, failure load tends to be governed by the material strength and the critical energy release rate has little effect on it. This is consistent with the conventional strength theories, since stress concentration and stress gradient at the corner are low in such a case. For sharp-corner specimens, failure strength is mainly controlled by the critical energy release rate. However, the material strength still has a minor effect on the failure load, because it governs the damage initiation and affects the damage zone size.

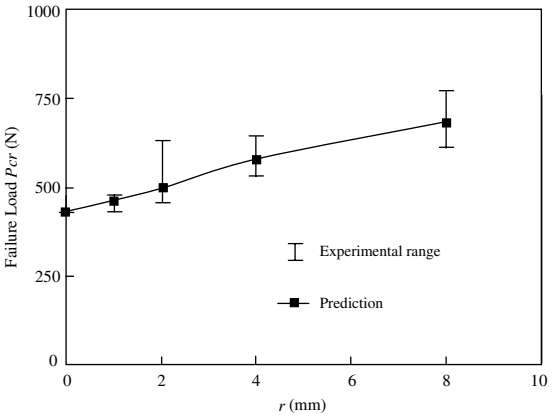

Fig. 12. Failure loads of channel sections.

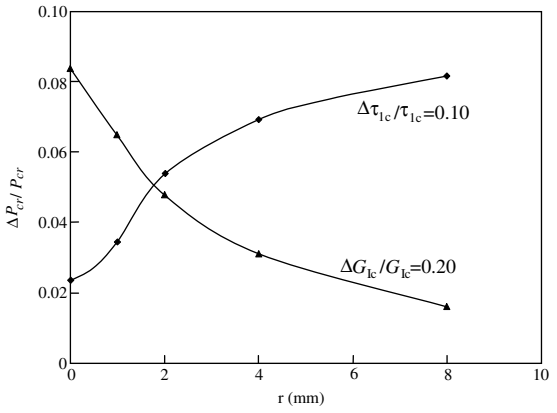

Fig. 13. Effect of corner radius on the sensitivity of failure strength to material strength and critical energy release rate.

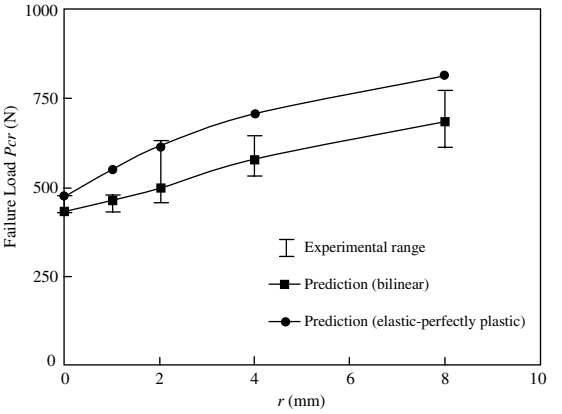

Fig. 14. Effect of interfacial constitutive curves on failure loads.

As mentioned in Section 1, several types of constitutive law have been used for the cohesive zone model in the literature. In this work, the bilinear curve ($n = 1$) in Fig. 2 has been used for all the analysis so far. To demonstrate the effect of different constitutive laws on the predictions, the 'elastic–perfectly plastic' curve ($n \to \infty$) was adopted to re-analyse the failure of channel-section specimens. The predictions are shown in Fig. 14, together with the experiments and those predicted by the bilinear law. Significant increase, around 20 percent, has been found in the predicted failure loads. When the 'elastic–perfectly plastic' curve is employed, the traction in the damage zone remains at a high level after damage initiation. This makes the damage zone much harder to open. Failure load is thus raised.

The above observation seems to be consistent with the general view that the bilinear curve would be more suitable for brittle materials, while the 'elastic–perfectly plastic' curve would be more suitable for ductile materials. However, it should be pointed out that the material strength used in this work was derived from bend tests which tend to give a higher value than that from simple tension. Taking this into account would mean that the predictions based on the 'elastic–perfectly plastic' curve were more representative. Further work is therefore required to establish which failure function is more suitable for nuclear graphite. Moreover, the choice of these functions for the constitutive law for irradiated graphite is likely to be different from that for unirradiated graphite. This topic is at present the subject of further investigation.

4. Conclusions

A failure model for nuclear graphite material, based on continuum damage mechanics, has been presented in this paper. Both the conventional stress-based and fracture-mechanics-based failure criteria are combined

into a single failure criterion. The model can predict crack initiation and propagation for structures under both regular and singular stress concentrations.

The numerical simulation and subsequent comparison with experiments on L-shape and channel-section specimens indicate that this failure model can be applied to graphite material. Although the model has to have a predefined crack path, this can be done satisfactorily with the performance of a linear stress analysis beforehand. Nuclear graphite appears to fail under the maximum principal stress, i.e. mode I failure. The linear stress analysis should therefore be performed to find out the location and direction of the maximum principal stress, which then allows the likely cracking site and crack growth path be introduced into the FE mesh.

Acknowledgements

The financial support of the Health and Safety Executive through contract NUC/56/60/5 is gratefully acknowledged. The authors are also grateful to B.C. Mitchell and J. Smart for providing their experimental data for comparison. The views expressed in this paper are those of the author(s) and do not necessarily represent the views of the Health and Safety Commission/Executive.

References

[1] J.E. Brocklehurst, in: P.L. Walker Jr., P.A. Thrower (Eds.), Chemistry and Physics of Carbon, vol. 13, Marcel Dekker, New York, 1977, p. 145.
[2] J.M. Whitney, R.J. Nuismer, J. Comp. Mater. 8 (1974) 253.
[3] P.P. Camanho, F.L. Mattews, Composites 28A (1997) 529.
[4] A. Sewweryn, Eng. Fract. Mech. 59 (1998) 737.
[5] M.L. Dunn, W. Suwito, Int. J. Solids Struct. 34 (1997) 3873.
[6] F. Costanzo, J.R. Walton, Int. J. Eng. Sci. 35 (1997) 1085.
[7] A. Pandolfi, P.R. Guduru, M. Ortiz, A.J. Rosakis, Int. J. Solids Struct. 37 (2000) 3733.
[8] H. Serizawa, M. Ando, C.A. Lewinsohn, H. Murakawa, J. Nucl. Mater. 283–287 (2000) 579.
[9] X.P. Xu, A. Needleman, J. Mech. Phys. Solids 42 (1994) 1397.
[10] E.D. Reedy, F.J. Mello, T.R. Guess, J. Comp. Mater. 31 (1997) 812.
[11] V. Tvergaard, J.W. Hutchinson, J. Mech. Phys. Solids 40 (1992) 1377.
[12] E. Smith, J. Mater. Sci. 32 (1997) 3939.
[13] E. Smith, Int. J. Fract. 95 (1999) 41.
[14] D.S. Dugdale, J. Mech. Phys. Solids 8 (1960) 100.
[15] Z. Zou, S.R. Reid, S. Li, J. Mech. Phys. Solids 51 (2003) 333.
[16] HKS, ABAQUS/Standard User's Manual, Version 6.2, 2001.
[17] Z. Zou, S.R. Reid, S. Li, P.D. Soden, J. Comp. Mater. 36 (2002) 477.
[18] Z. Zou, S.R. Reid, S. Li, P.D. Soden, Comp. Struct. 56 (2002) 375.
[19] B.C. Mitchell, J. Smart, S.L. Fok, B.J. Marsden, J. Nucl. Mater. 322 (2003) 126.
[20] J. Smart, in: M.H. Aliabadi, C.A. Brebbia, D.J. Cartwright (Eds.), Proceedings of the first International Conference on Computer Aided Assessment & Control of Localised Damage, vol. 3, Computational Mech., 1990, p. 185.